Beyond Shape Engineering of TiO2 Nanoparticles: Post-Synthesis Treatment Dependence of Surface Hydration, Hydroxylation, Lewis Acidity and Photocatalytic Activity of TiO2 Anatase Nanoparticles with Dominant 001 or 101 Facets

Beyond Shape Engineering of TiO_2 Nanoparticles: Post-Synthesis Treatment Dependence of Surface Hydration, Hydroxylation, Lewis Acidity and Photocatalytic Activity of TiO_2 Anatase Nanoparticles with Dominant {001} or {101} Facets

Lorenzo Mino,[a*+] Francesco Pellegrino,[a+] Steffi Rades,[b] Jörg Radnik,[b] Vasile-Dan Hodoroaba,[b] Giuseppe Spoto,[a] Valter Maurino,[a] Gianmario Martra[a]

[a]Department of Chemistry and NIS Centre, University of Torino, via Giuria 7, 10125 Torino, Italy
[b]BAM Federal Institute for Materials Research and Testing, 12205 Berlin, Germany
[+]These authors contributed equally to this work

Corresponding Author
*E-mail: lorenzo.mino@unito.it

Abstract
TiO_2 anatase nanoparticles are among the relevant players in the field of light-responsive semiconductor nanomaterials used to face environmental and energy issues. In particular, shape-engineered TiO_2 anatase nano-sheets with dominant {001} basal facets gained momentum because of the possibility to exploit different and/or improved functional behaviors with respect to usual bipyramidal TiO_2 anatase nanoparticles, mainly exposing {101} facets. Nevertheless, such behavior depends in a significant extent on the physico-chemical features of surfaces exposed by nano-sheets. They can vary in dependence of the presence or removal of capping agents, namely fluorides, used for shape-engineering, and experimental investigations in this respect are still a few. Here we report on the evolution of interfacial/surface features of TiO_2 anatase nano-sheets with dominant {001} facets from pristine nanoparticles fluorinated both in the bulk and at their surface, to nanoparticles with F^- free surfaces by treatment in a basic solution and to totally F^- free nanoparticles by calcination at 873 K. The nanoparticles fluorine content and its subsequent evolution is determined by complementary techniques (ion chromatography, ToF-SIMS, XPS, AES, SEM-EDX), probing different depths. In parallel the evolution of the electronic properties and the Ti valence state is monitored by UV-Vis spectroscopy and XPS. The calcination treatment results in {001} facets poorly hydroxylated, hydrated and hydrophilic, which appear as surface features consequent to the expected (1x4) reconstruction. Moreover, IR spectroscopy of CO adsorbed as probe molecule indicates that the Lewis acidity of Ti^{+4} sites exposed on (1x4) reconstructed {001} facets of calcined TiO_2 nano-sheets is weaker than that of cationic centers on {101} facets of bipyramidal TiO_2 anatase nanoparticles. The samples have also been tested in phenol photodegradation highlighting that differences in surface hydration, hydroxylation and Lewis acidity between TiO_2 nanoparticles with nano-sheet (freed by F^- by calcination at 873 K) and bipyramidal shape have a strong impact on the photocatalytic activity, that is found to be quite limited for the nanoparticles mainly exposing (1x4) reconstructed {001} facets.

Keywords: shape-controlled TiO_2 nanoparticles, F^- doping, Ti^{3+}, H_2O adsorption, CO adsorption, phenol photodegradation.

1. Introduction

In the last years semiconductor functional materials have attracted increasing attention for their widespread environmental and energy applications.[1-2] In these fields crystal facet engineering of semiconductors nanoparticles (NPs), in particular of TiO_2, is emerging as an important strategy to finely tune their physicochemical properties to optimize surface reactivity and selectivity.[3-5] For anatase TiO_2, the most widely employed semiconductor photocatalyst, the shape under equilibrium conditions predicted by the Wulff construction is a truncated tetragonal bipyramid, mainly exposing the {101} surfaces. However, starting from the seminal paper by Yang *et al.*,[6] several researchers tried to obtain TiO_2 anatase nano-sheets (n-sh) with extended basal {001} surfaces, that have been proposed to possess superior photocatalytic activity.[7-8] Since the {001} surfaces have a high surface energy**,** the preparation of TiO_2 n-sh requires the use of suitable adsorbates which can substantially lower their surface energy.[9] In this respect, hydrofluoric acid is the most commonly employed capping agent since fluoride ions can preferentially adsorb and stabilize the {001} facets.[9] After the hydrothermal synthesis, the surface of the anatase TiO_2 n-sh is thus terminated with Ti–F groups and F^- ions are expected to be present also in the bulk of the NPs. In some studies, as-prepared TiO_2 n-sh are used in photocatalytic reactions without further treatments,[10] hindering the possibility to distinguish between the role of {001} surfaces and the electronic states resulting from the presence of bulk and surface fluorides. Indeed, it has been demonstrated that fluorides adsorption strongly affects interfacial hole and electron transfer in photocatalysis, as well as the extent of adsorption of substrates and O_2. This results in the modification of the mechanism and rate of substrate oxidation,[11-12] as well as in the rate of O_2 reduction and carrier recombination.[13] Moreover, also surface hydrophilicity is modified.[14]

To specifically investigate the effect of {001} facet engineering, fluorides must be thus removed and the common procedure is calcination at 873 K. Thermal treatments at lower temperatures (i.e. 773 K) were not completely effective in this respect.[15] DFT calculations highlighted that such high temperature treatment should induce (1x4) reconstruction of TiO_2 (001) surfaces , that, conversely to what claimed for as-prepared TiO_2 n-sh particles, apparently leads to a weak reactivity.[16] The atomic

structure and reconstruction mechanism at elevated temperatures was recently investigated by *in situ* spherical aberration corrected scanning transmission electron microscopy,[17] but, at the best of our knowledge, experimental insights, at the molecular level, on the evolution of surface chemical features of anatase TiO_2 n-sh from the pristine fluorinated to the bulk and surface F^- free form obtained by calcination, are lacking. Moreover, the effect of the substitution of only surface fluorides of TiO_2 n-sh with OH^- by washing with a basic solution (of NaOH, in the present case) is also of interest.

In this respect, here we report a contribution to the elucidation of three aspects of TiO_2 n-sh in their pristine, surface F^- free and bulk and surface F^- free forms thought to be relevant for the surface and interfacial behavior of titania nanoparticles as photocatalysts: (i) hydroxylation (by mid-IR spectroscopy in controlled atmosphere); (ii) hydration (by both microgravimetry and mid- and near –IR spectroscopy of adsorbed water), which plays a significant role in photocatalytic processes at titania surfaces, not only in liquid-solid regime, but also in gas-solid regime in ambient air;[18-19] and (iii) Lewis acidity of Ti^{4+} surface sites, as probed by IR spectroscopy of adsorbed CO. For the sake of comparison, truncated bipyramidal anatase TiO_2 nanoparticles, mainly exposing {101} facets,[20] were also considered. To strengthen the comparative analysis of the surface features of TiO_2 n-sh in dependence on the F^- removal treatments and with respect to truncated bipyramidal TiO_2 NPs, combined structural (by X-ray diffraction), textural (in terms of specific surface area) and morphological (by both scanning and high-resolution transmission electron microscopy, SEM and HRTEM, respectively) investigations were carried out, targeting in particular the relative amount of {001} and {101} facets exposed by TiO_2 n-sh. Indeed, the interface and relative amount of co-exposed {001} and {101} facets have been reported to crucially influence the physico-chemical and functional properties.[21-22] Moreover, special care was devoted to monitor the evolution of the F^- content. On one hand, quantitation was pursued by complementary techniques as chemical analysis of dissolved samples and of washing solutions, and analytical inspection at different depth in the TiO_2 nanoparticles by energy X-ray dispersive spectroscopy (EDX) coupled to SEM, Auger electron spectroscopy (AES), X-ray photoelectron spectroscopy (XPS) and time-of-flight secondary ion mass spectrometry (ToF-SIMS). On the other

hand, the fading by fluoride removal of electronic states due to the presence of bulk and surface F^- ions was monitored by diffuse reflectance UV-Vis-NIR and mid-IR transmission spectroscopy. Moreover, the evolution of the Ti valence state has been investigated by XPS.

The differences in surface chemical features of TiO_2 nanosheets freed from both bulk and surface fluorides by calcination, mainly terminated by {001} (1x4) reconstructed surfaces, and truncated bipyramidal TiO_2 nanoparticles mainly exposing {101} facets are also discussed in terms of performance in the photocatalytic degradation of phenol, one of the most studied substrate in photocatalysis and with known degradation mechanisms.[23-24]

2. Experimental

2.1 Preparation of TiO_2 nanoparticles

TiO_2 nano-sheets. The preparation of TiO_2 nano-sheets was carried out with a solvothermal method following an established literature procedure.[25-26] In a typical synthesis 25 ml of $Ti(OBu)_4$ (Aldrich reagent grade 97%) was poured in a 150 ml Teflon lined stainless steel reactor and 3.5 ml of concentrated hydrofluoric acid (Aldrich reagent grade 47%) was added dropwise under stirring. The reactor was sealed and kept under stirring at 523 K for 24 hours. The resulting bluish paste was centrifuged and washed with acetone to remove the residual organics and then with water (Milli-Q). Finally, the obtained aqueous suspension was freeze-dried obtaining a bluish powder. The sample in this form is labelled as TiO_2 n-sh throughout the text.

To attain the removal of the fluorides from the surface, the as-prepared TiO_2 n-sh was washed with 0.1 M NaOH (10 mg TiO_2/ml, 2 hours under stirring at ~300 K).[14] The suspension was then centrifuged (5000 rpm, 15 min), and the supernatant kept for quantification of fluorides and possibly solubilized Ti species, by ion chromatography and ICP-MS, respectively. The paste of TiO_2 nanoparticles recovered by centrifugation and then again centrifuged in 0.1 M HNO_3 (40 ml, 5000 rpm, 15 min) and ultrapure water (MilliQ, Millipore; 40 ml, 5000 rpm, 15 min) to remove Na^+ ions from the surface. The

effectiveness of this treatment was assessed by Auger electron spectroscopy and ToF-SIMS analyses (*vide infra*). The sample resulting from these treatments is hereafter referred to as TiO_2 n-sh_NaOH.

The removal of the fluorides from both the bulk and the surface of TiO_2 n-sh was achieved by calcination in air at 873 K. In a typical treatment, 200 mg of TiO_2 n-sh powder were heated up to 873 K at 6.5 K/min, kept for 60 min at the indicated temperature, and then cooled down to RT in the closed furnace in approximately 10 hours. This sample will be hereafter referred to as TiO_2 n-sh_873K.

Truncated bipyramidal TiO_2 nanoparticles. The material named TiO_2 bipy NPs were obtained by forced hydrolysis of 40 mM aqueous solution of $Ti(TeoaH)_2$ complex (TeoaH = triethanolamine; initial pH 10), carried out by hydrothermal treatment at 453 K for 90 hours in autoclave. This procedure is similar to that developed by Sugimoto, but without the intermediate gelation step.[27] Further details on the preparation of these NPs, hereafter referred to as TiO_2 bipy, which show a bipyramidal shape, mainly limited by {101} facets, can be found in our previous publication.[20]

Scheme 1. Synthesis of TiO_2 nano-sheets and TiO_2 bipyramidal nanoparticles.

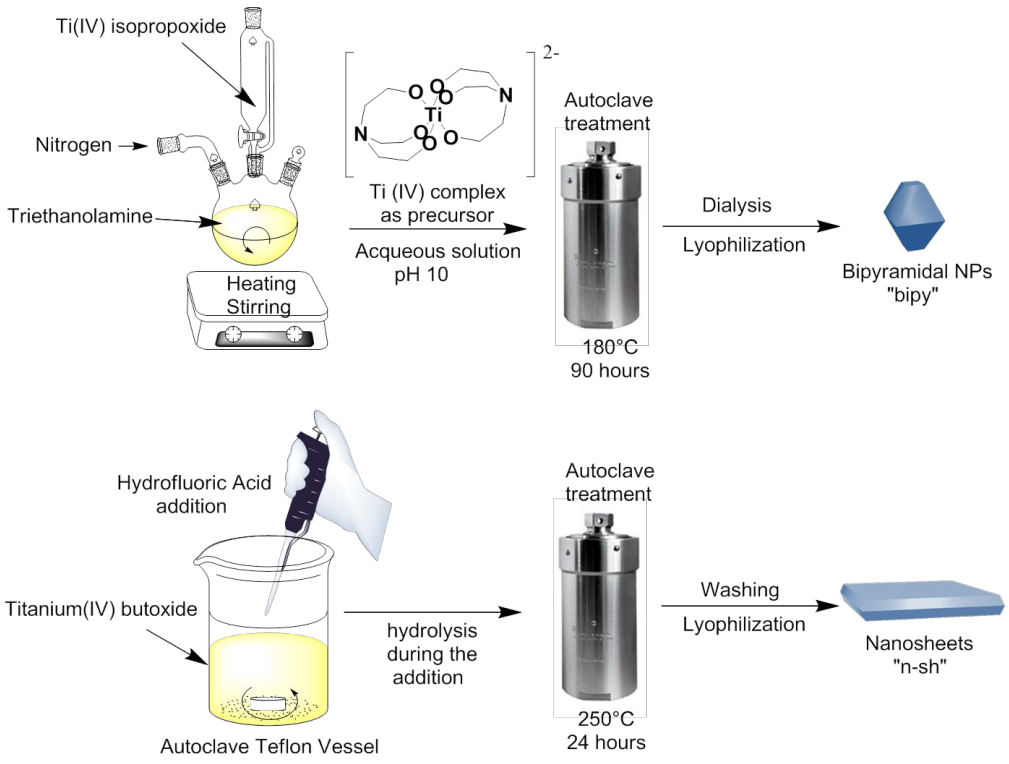

2.2 Characterization methods

High resolution transmission electron microscopy (HR-TEM) images of the materials (powder grains "dry" dispersed on lacey carbon Cu grids) were obtained using a JEOL 3010-UHR microscope operated at 300 kV.

Adsorption of N_2 at 77 K was exploited to measure the specific surface area of the samples with a Micromeritics ASAP 2020 sorption analyzer. Before the measurements samples were outgassed at r.t., until the attainment of a residual pressure of 1×10^{-3} mbar. Data were treated by applying the Brunauer–Emmett–Teller (BET) equation.

X-ray powder diffraction patterns of the various types of TiO_2 nanoparticles were recorded with a PANalytical X'Pert Pro powder diffractometer, equipped with an X'Celerator detector, using Cu K_α radiation generated at 45 kV and 40 mA. The 2θ range was from 10° to 80°with a step size of 0.01° and a counting time of 0.6 s per point. The 004 and 200 anatase reflections were considered to calculate the average size of crystal domains (d) along the [001] and [100] directions, respectively, by the Scherrer equation: $d = \frac{K\,\lambda}{(B_{exp}-B_{ins})cos\theta}$

were K is a shape factor (assumed to be 0.9 in the present case), λ is the X-ray wavelength, θ is the measured Bragg angle, B_{exp} and B_{ins} are the experimental and instrumental broadening, respectively. The instrumental broadening was evaluated using a Si powder standard.

IR spectroscopy in controlled atmosphere. An aliquot of each type of TiO_2 nanoparticles was pressed in self-supporting pellets ("optical density of ca. 10 mg·cm^{-2}) and placed in quartz cells equipped with KBr windows designed to carry out spectroscopic measurements at the beam temperature (b.t.; ca. 323 K) or at low temperature (i.e. ~100 K) by cooling with liquid N_2.[20] The cells were connected to a conventional vacuum line (residual pressure: 1×10^{-5} mbar) allowing all thermal treatments and adsorption-desorption experiments to be carried out *in situ*. A Bruker IFS 28 spectrometer (resolution: 2 cm^{-1}; detector: MCT) was employed for the spectra collection at b.t and at ca. 100 K, averaging 128 scans. H_2O and D_2O (99% D atoms, Eurisotop) were introduced onto the

samples after several freeze-pump-thaw cycles. To attain a complete H/D isotopic exchange of surface hydroxy groups and water molecules, admission (15 mbar)/outgassing (residual pressure as low as $\times 10^{-5}$ mbar) of D_2O vapor was repeated until invariance of spectra. For CO adsorption, the samples were previously outgassed at 873 K for 120 min and contacted with 20 mbar of O_2 at the same temperature. Then, the pellets were cooled to 373 K in O_2 and then cooled to r.t. under outgassing. Finally, they were cooled down to *ca*. 100 K by filling with liquid N_2 a reservoir in contact with the sample holder trough a metallic seal. For the collection of the spectra of CO adsorbed at 60 K, the self-supporting pellets were activated as described above in a properly modified Oxford CCC 1204 cryostatic chamber, inserted in a Bruker Equinox 55 spectrometer (resolution: 2 cm^{-1}; detector: MCT; 128 scans).

Diffuse reflectance (DR) UV-Vis-NIR spectra were recorded with a Cary 5000 Varian spectrophotometer equipped with an integrating sphere with an inner coating of Spectralon®. This material was used also as reference. For the collection of spectra, thick self-supported pellets of TiO_2 nanoparticles were placed in a cell with an optical quartz window designed to carry out the measurements in controlled atmosphere, by connection to a conventional vacuum line (as for IR spectroscopy). For the sake of clarity, the spectra are reported only in the 380-2500 nm range, starting, on the short wavelength side, from the onset of the edge-shaped inter-gap absorption typical of TiO_2 anatase,[28] extended towards the UV, which dominates the spectral profile by far.

Determination of fluoride by ion chromatography. In order to evaluate the total amount of fluorides a complete mineralization in microwave was performed heating the samples for 90 min at 473 K under vigorous stirring in NaOH 10 M. After the treatment, a dilution 1:10 of the solution was analyzed by Ion Chromatography (IC). The instrument (DIONEX DX 500) is equipped with a GP40 pump, AS9-HC column (Dionex, length 25 cm and internal diameter of 4 mm), Suppressor ASRS-Ultra II autosuppression mode, electrochemical detection system ED40, LC30 column thermostat (temperature 303 K). The mobile phase consists of 9 mM K_2CO_3 and the eluent flow is equal to 1 mL min^{-1}.

Determination of soluble Ti species by ICP-MS. Inductively Coupled Plasma – Mass Spectrometry (ICP-MS) analyses were carried out using a Thermo Scientific ICP-MS ICAP-Qs model, equipped with a quadrupole mass analyzer and a flatpole quadrupole collision/reaction cell. The instrument is calibrated with 1% nitric acid standard for Ti prepared by diluting standard reference certificates at 1000 mg L^{-1} using ^{45}Sc, ^{89}Y, ^{159}Tb (100 ppb) as internal standards. The calibration curve was constructed with 5 points and linear correlation coefficient > 0.99. Interference due to polyatomic ions is eliminated by operating the collision cell in He mode with kinetic energy discrimination (He - KED). ^{48}Ti was used for quantitation.

SEM/EDX. For SEM and EDX measurements aluminum holders were used, which were cleaned by sonication in ethanol and subsequently sample powder was pressed on the Al-holder with spatula. High-resolution electron micrographs and EDX spectra have been collected with a SEM of type Zeiss Supra 40 (Carl Zeiss, Oberkochen, Germany), equipped with a Schottky field emitter and having attached a silicon drift detector energy dispersive X-ray spectrometer (SDD-EDS) from Thermo Fisher Scientific (energy resolution at Mn Kα of 128 eV and 100 mm^2 crystal active area). SEM images were acquired operating the microscope at 10 kV.

Auger electron spectroscopy (AES). The powder was deposited on a cleaned Si-wafer (sonicated in isopropanol) by slightly pressing the powder with a spatula on the wafer surface. AES analysis was carried out with a PHI 700 Auger Scanning Probe (ULVAC-PHI Inc.) equipped with a coaxial cylindrical mirror analyzer. Auger electrons spectra were excited by the primary electron beam at different locations on the sample surface. To evaluate the presence of Fluorine on the TiO_2 nanoparticles surface, AES survey spectra as well as window spectra of energy region corresponding to F KLL were recorded (5 keV, 20 nA and 20 keV, 1 nA).

X-ray photoelectron spectroscopy (XPS). The XPS investigations were performed with a KRATOS Axis Ultra DLD. Monochromated Al Kα with an energy of 1486.6 eV was used for the excitation of the photo- and Auger electrons. The binding energy scale of the spectra were referred to C1s at 285 eV. Quantitative analysis was performed with Casa XPS software package using the background-

corrected area of the main peaks of the elements and sensitivity factors and the spectrometer-specific transmission function. The peaks were fitted with a Gaussian-Lorentzian profile.

Time-of-flight secondary ion mass spectrometry (ToF-SIMS). Samples were prepared on silver foil as well as on silicon wafers by slightly pressing the powder with a spatula on the wafer surface. The substrates were cleaned by sonication in isopropanol prior to sample deposition. ToF-SIMS measurements were performed on a ToF-SIMS IV instrument (ION-TOF GmbH) of the reflectron type, equipped with a 25 keV bismuth liquid metal ion gun as a primary ion source.

Photocatalytic activity assessment. The photocatalytic activity of TiO_2 was evaluated by irradiating the suspensions of titania nanoparticles (loading 100 mg l^{-1}; pH=6.5) in cylindrical Pyrex glass cells under magnetic stirring (4 cm diameter, 2.5 cm height, area of 1.26 x 10^{-3} m^2, cut-off 295 nm, 5 ml suspension volume), using a fluorescent source with λ_{max} = 365 nm (Philips PL-S 9W BLB, integrated irradiance = 10 W m^{-2}). Substrate absorption at this wavelength is negligible. The use of this wavelength assures minimal impact of nanoparticle agglomeration on photoactivity during the test.[24] Moreover, to mitigate the influence of large agglomerates formation during the experiment, the irradiation time was limited to less than one half-life of phenol. Photocatalytic activity was measured as the initial rate of phenol phototransformation, by fitting disappearance curves to an exponential decay. Incident radiant power was measured in the range 290-400 nm with an Oceans Optics USB2000 spectrophotometer equipped with a cosine corrected optical fiber probe, spectroradiometrically calibrated with a NIST traceable DH-2000 CAL UV-Vis source (Ocean Optics). The initial concentration of phenol is 0.1 mM. Time profiles of phenol decay where obtained as average of three irradiation runs.

HPLC determination of phenol has been carried out with an Agilent Technologies HPLC chromatograph 1200 Series equipped with a diode array detector, binary gradient high-pressure pump and an automatic sampler. Isocratic elution was carried out with a mixture of 15/85 acetonitrile/formic acid aqueous solution (0.05 % w/v), flow rate 0.5 ml min^{-1}, injection volume 20 µl. The column used was a Kinetex C18 150-2 (150 mm length, 2 mm I.D., 2.6 µm core-shell particles, Phenomenex).

3. Results and discussion

3.1 Structural and morphological characterization of the TiO_2 nanoparticles

Figure 1A shows a representative SEM image of the as-prepared TiO_2 n-sh, appearing as sheets 75 ± 25 nm wide in the basal plane and 9 ± 1.6 nm thick (see Table 1). In HR-TEM images (Figure 1B), nanoparticles properly oriented with respect to the impinging electron beam show lattice fringes 0.2370 nm apart (d_{004}= 0.2378 nm, ICDD PDF 00-021-1272) parallel to the lateral view of the basal facets, and related FT (inset) confirm that these facets are normal to the *c*-axis (reported in the image) and thus correspond to {001} surfaces. The lateral boundaries of the nanoparticle imaged in Figure 1B form an angle of ~130°. This is compatible with the projection of intersecting (101) and $(10\bar{1})$ surfaces for a NP with the *a*-axis forming a small angle with the image plane since the angle between intersecting (101) and $(10\bar{1})$ surfaces should be 136°, considering a tetragonal unit cell with lattice parameters a = 3.78 Å and c = 9.51 Å. The TiO_2 n-sh_NaOH sample, resulting from the washing of TiO_2 n-sh in a NaOH solution to remove surface fluorides shows a similar morphology (see Figure 1C and Figure S1 in the Supporting Information), that, conversely, was almost lost by subsequent calcination at 873 K (Figure 1D). Therefore, the calcined TiO_2 n-sh_NaOH will no longer be considered. Noteworthy, direct calcination of TiO_2 n-sh does not lead to significant morphological changes (sample TiO_2 n-sh_873K), as from both SEM and HR-TEM imaging (Figure 1E and 1F, respectively).

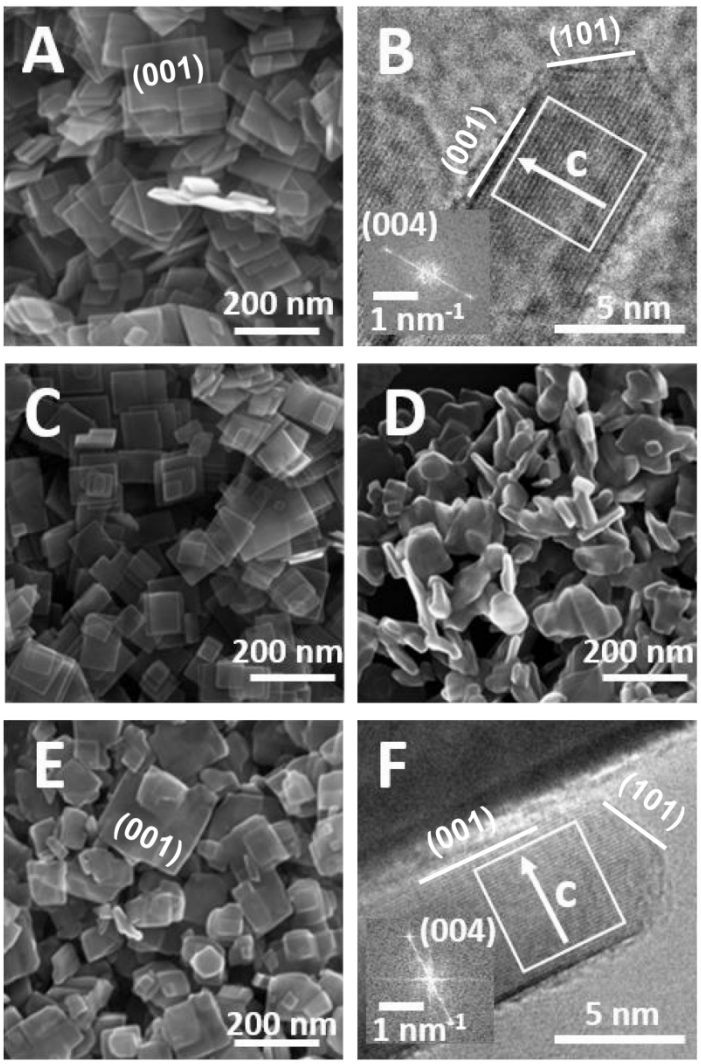

Figure 1. SEM (panels A,C,D,E) and HR-TEM (panels B,F; inset: FT of the image portion within the with frame) images of: A,B) as-prepared TiO_2 n-sh; C) TiO_2 n-sh _NaOH; D) TiO_2 n-sh _NaOH calcined at 873 K; E,F) TiO_2 n-sh _873 K.

Figure 2A shows a representative SEM image of the as-prepared TiO_2 bipy, which appear as truncated bipyramids 30 ± 5 nm wide in the basal plane and 40 ± 9 nm thick along the *c*-axis (see Table 1). In the HR-TEM image (Figure 2B) we can see in greater detail a single particle with well-defined borders, which appears as a bidimensional projection of a truncated bipyramid with the *c*-axis almost perpendicular to the electron beam. From the SEM and HR-TEM images reported in Figure 2C-D we can see that calcination at 873 K does not induce significant morphological changes.

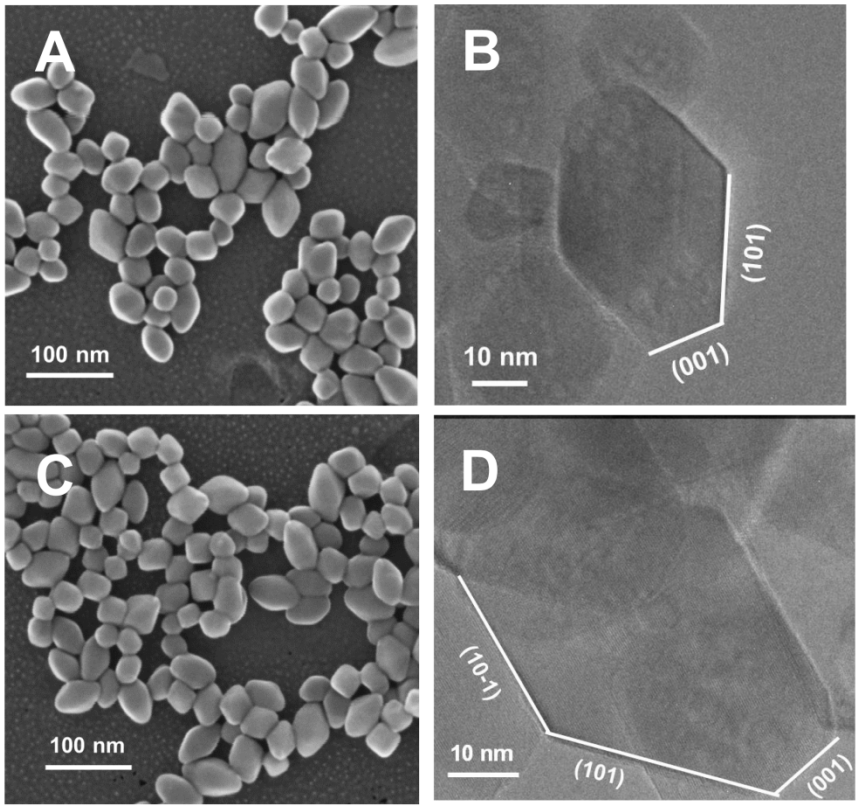

Figure 2. SEM (panels A, C) and HR-TEM (panels B, D) images of: A,B) TiO_2 bipy and C,D) TiO_2 bipy_873 K.

All samples were found to be pure anatase TiO_2 phase by XRD (Figure S2). No significant variations of lattice parameters due to the incorporation of F^- were observed. The Scherrer analysis, applied as an integral method, highlights that the average crystallite dimension in the [001] direction is approximately doubled for TiO_2 n-sh_873K with respect to TiO_2 n-sh and TiO_2 n-sh_NaOH (Table 1), suggesting that the primary nanosheets might have aggregated in pairs along the *c*-axis, as schematized in Figure S3. This stacking through basal facets should be the responsible for the decrease of the specific surface area (SSA_{BET}) from 53 to 34 m^2/g, because no significant change in size and shape of primary nanoparticles was observed neither in SEM nor in HR-TEM images. Conversely, very limited changes in crystal size along the [001] direction and in SSA_{BET} occurred for TiO_2 bipy when passing from the pristine to the calcined at 873 K form, in agreement with the electron microscopy results (Figure 2). The pairing of nano-sheet particles, which has been already proposed in previous studies,[29]

should have a relevant impact on the relative amount of lateral {101} and basal {001} surfaces of TiO_2 n-sh_873K. By a geometric modeling of nano-sheet pairing (details in Figure S4 and related comment), the {101}:{001} ratio was estimated to change on an average from 20:80 for TiO_2 n-sh to 40:60 for TiO_2 n-sh_873K (Table 1). The resulting relative change in calculated specific surface area was in excellent agreement with the experimental one (see SI for details).

Table 1. Average dimension of crystal domains obtained by Scherrer analysis of the 004 and 200 XRD peaks, particle thickness (T) and basal length (L) measured from SEM images, specific surface area and relative change, calculated average percentage of {001} facets and relative change in SSA (see SI for calculation details).

Sample	d_{004} (nm)	d_{200} (nm)	T (nm)	L (nm)	SSA_{BET} (m^2/g)	SSA_{BET} relative change	calculated %{001}	calculated SSA relative change
n-sh	18	> 100	9.4 ± 1.6	75 ± 25	53	1	78	1
n-sh_NaOH	21	> 100	8.4 ± 1.7	73 ± 27	57	~1	79	1
n-sh_873K	46	> 100	10 ± 2	64 ± 25	34	0.64	58	0.62
bipy	36	29	40 ± 9	30 ± 5	43	1	10	-
bipy_873K	32	26	35 ± 5	45 ± 9	37	0.86	13	-

3.2 Determination of the F^- content

The fluorine content and its subsequent evolution were determined by complementary techniques (Table 2), also probing different depths (details in Figure S5 and related comment). By ion chromatography, pristine TiO_2 n-sh is found to contain 16 mg F^-/g TiO_2, decreasing to 7 mg F^-/g TiO_2 for TiO_2 n-sh_NaOH, where ion-exchange is expected to remove fluorides only from the surface. The absence of significant dissolution of surface layers was confirmed by the trace amount of titanium found in the supernatant, corresponding to less than 0.015 atoms of Ti for nm^2 of TiO_2. As a result, an initial F^- surface concentration of ~5 F^-/nm^2 is calculated. This surface fluorination is relevant since the Ti^{4+} density is 7 and 5 nm^{-2} on {001} and {101} surfaces, respectively.[30] The significant decrease in

the ToF-SIMS signal of F^- in the mass spectra of TiO_2 n-sh_NaOH sample, normalized to the TiO_2^- intensity, and in the XPS F1s spectra, normalized to the Ti2p signal, (see Table 2) supports partial removal of fluorine as found with IC, i.e. by 'losing' F^- ions from the outermost surface of nano-sheets particles by ion exchange. Note that AES (probing 3-4 nm depth, i.e. reaching the bulk of the NPs which are ~ 9 nm thick) as well as EDX (probing ~1 μm depth) cannot distinguish between the levels of fluorine signals as detected in the two samples TiO_2 n-sh and TiO_2 n-sh_NaOH (details in the SI). By combining these results, one can thus infer that TiO_2 n-sh_NaOH does not contain F^- ions on its surfaces, while they are still present in the bulk (Figure S3). A reliable quantification into absolute chemical composition of fluorine with all four techniques, ToF-SIMS, XPS, AES and EDX is impossible mainly due to the strong morphological effects typical for nanopowders (heterogeneous distribution of solids/voids, heterogeneous orientation of nanoparticles, see SI).[31]

All methods agreed in indicating the removal of fluorine in the nano-sheets calcined at 873 K down to or below the detection level of each method (see Table 2), from both the bulk and the surface.

Table 2. Fluoride concentration for the different samples obtained by ion chromatography, and fluorine signals as detected by ToF-SIMS, XPS, AES and EDX.

Sample	IC (mg F^-/g TiO_2)	ToF-SIMS I_{F^-}/I_{TiO2^-} (a. u.)	XPS I_F/I_{Ti} (a. u.)	AES $I_{F\ KLL}$ (a. u.)	EDX $I_{F\ K\alpha}$ (a. u.)
n-sh	16.1 ± 1.2 (5 F^-/nm^2)*	73 ± 6	0.20 ± 0.04	Yes	Yes
n-sh_NaOH	7.0 ± 0.8	54 ± 4	0.05 ± 0.02	Yes	Yes
n-sh_873K	< 0.4	3.6 ± 0.4**	0.03 ± 0.01	≅LoD	≅LoD
bipy	< 0.4	5.7 ± 0.6**	≅LoD***	≅LoD	≅LoD

* F^- surface density, see text for details

**This concentration level, different from zero also for the originally F-free TiO_2 bipy, was found even in the Si (100) blank substrate used for analysis, demonstrating that this level of F^- represents the background contamination present at the ToF-SIMS instrument used. For detailed explanation of the results in Table 2 please consult the SI (sections EDX, AES, XPS and ToF-SIMS). LoD= limit of detection

***At this low level F is detectable, but not reliably quantifiable, see also SI

The calcination process has also a strong impact on the electronic properties of the pristine F^- containing nanoparticles. Indeed, the electronic spectrum of TiO_2 n-sh (Figure 3A) shows a very broad electronic absorption spread over the 600-2500 nm range, due to trapped excess electrons resulting from the substitution of O^{2-} ions by F^- ions.[32-34] Most part of this absorption is still present in the spectrum of TiO_2 n-sh_NaOH. Moreover, in the MIR spectral range (Figure 3B) these samples show a spectral profile resulting from the superimposition of a continuous increase in absorbance, from 2500 up to 10000 nm (spectral cutoff due to bulk Ti−O vibrations), and of a series of minor localized signals, vibrational in nature. The latter will be commented on in the following, while the first one is typical of free conduction band and shallow-trapped electrons.[10, 35-36] After calcination, the spectral features in the overall 600-10000 nm (panels A+B of Figure 3) due to electronic defects associated with the presence of F^- disappear, confirming that fluorine has been completely removed.

We performed also a parallel XPS analysis to investigate the evolution of the valence states. In the Ti2p XPS spectra reported in Figure S10 we can identify a specific component of the $Ti^{4+}2p_{3/2}$ at 459.9 eV ascribed to the influence of the F^- anions.[37-38] The intensity ratio between this Ti^{4+} component and the main $Ti^{4+}2p_{3/2}$ signal decreased from 0.3 for TiO_2 n-sh to *ca.* 0.1 for the other samples (see SI for the details), in agreement with the evolution of the electronic properties highlighted by UV-Vis-NIR-MIR spectroscopy and with the progressive decrease of F^- content (see Table 2). A contribution of Ti^{3+} to the Ti2p signal can be also present, especially for the TiO_2 n-sh sample (see SI).[39]

Finally, for the bare TiO_2 nanoparticles we calculated the band gap using a Tauc plot (Figure S11) to evaluate the impact of the different exposed facets. The results are 3.10 ± 0.07 eV for TiO_2 bipy and 3.26 ± 0.06 eV for TiO_2 n-sh_873K. These data seem to be in contradiction with experimental results on micrometric crystals[40] and with DFT calculations which reported a smaller band gap for the {001} facets. However, it should be considered that the particle thickness for TiO_2 n-sh_873K is below 10 nm, while it is about 40 nm for TiO_2 bipy (see Table 1), therefore the higher band gap for nano-sheet particles could be also due to quantum confinement effects which have been reported to play a role for anatase nanoparticles up to 15 nm in diameter.[41] Anyhow, these small differences in band gap should

not impact our tests of the photocatalytic activity which are performed under pure UV irradiation at 3.4 eV (see section 3.5).

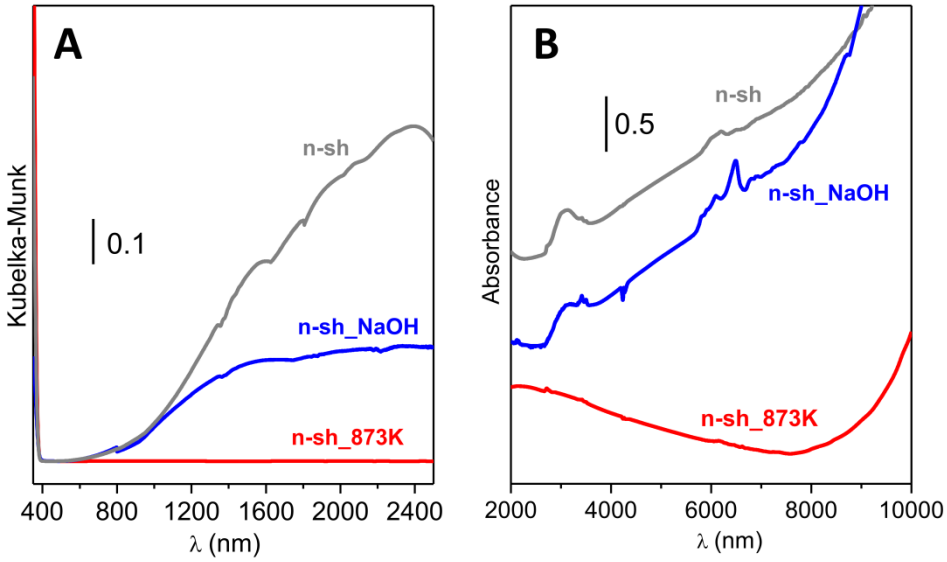

Figure 3. Diffuse reflectance spectra, in the 380-2500 nm range and in Kubelka-Munk units (A), and transmission NIR-MIR spectra, in the 2000-10000 nm range and in absorbance units (B) of TiO_2 n-sh, TiO_2 n-sh_NaOH and TiO_2 n-sh_873K. On the X-axis of panel B, where spectra in the MIR range are shown, wavelength values are reported, instead than conventional wavenumber values, for the sake of consistency with spectra in panel A (being wavelength values commonly used for electronic spectra in the UV-Vis-NIR ranges). Note on the MIR spectrum of TiO_2 n-sh_873K: the apparent decrease in absorbance from 8000 to 2000 nm is the typical effect of decreased scattering of the samples at higher wavelengths, observed when measuring the spectrum in transmission, instead of in diffuse reflectance.

3.3 Surface hydration and hydroxylation

The interaction between water and fluorinated (TiO_2 n-sh) and F^- free (TiO_2 n-sh_NaOH and TiO_2 n-sh_873K) was investigated by measuring the amount of H_2O molecules that can be reversibly adsorbed at room temperature (r.t) (Figure 4A). This amount depends on the adsorptive properties of the "first hydroxylation/hydration layers", constituted by surface hydroxy groups and strongly adsorbed water which are not desorbed by outgassing at r.t. (*vide infra*). Pristine TiO_2 n-sh adsorbs up to ~8 H_2O molecules/nm^2 when in contact with H_2O at 15 mbar. The removal of F^- by the two different methods impacts in two opposite directions the surface hydrophilicity: for TiO_2 n-sh_NaOH, the substitution of surface F^- by exchange with OH^- results in an increase to ~12 H_2O molecules/nm^2, whereas for calcined TiO_2 n-sh_873K the water adsorption capacity becomes limited to only ~5 H_2O

molecules/nm^2. This finding is in agreement with DFT calculations which suggested that in the terrace region of the (1×4) reconstructed (001) surface, which should be obtained after calcination, water is physisorbed or not adsorbed at all.[16] It is worth mentioning that TiO_2 bipy, overwhelmingly exposing {101} surfaces, adsorbs up to ~10 H_2O molecules/nm^2. For TiO_2 n-sh_873K, where these facets account on an average for 40% of the surface, the actual amount of H_2O molecules adsorbed on fluorine free calcined {001} terminations might be of the order of ~2 H_2O molecules/nm^2. A similar consideration holds for TiO_2 n-sh_NaOH, which exposes on average 20% of {101} facets, but in this case the F^- free unreconstructed {001} surface exhibits an affinity towards water similar or slightly higher that the {101}. No definitive conclusions can be derived for the pristine TiO_2 n-sh since F^- can modify also the properties of {101} surfaces.[14]

The amount of H_2O per nm^2 reversibly adsorbed on TiO_2 bipy in contact with H_2O at 15 mbar might correspond to the formation of 2 molecular layers, adsorbed on the first hydration layer, assuming an average density of ~5.3 molecules/nm^2 for each of the three layers, on the basis of molecular dynamic calculations of H_2O on a TiO_2 anatase (101) surface,[42-43] (details on the calculations in the SI). For H_2O on (001) TiO_2 anatase, a radial distribution function was found only for an unreconstructed hydroxy-free surface,[42] resulting in an average density of ~9.3 molecules/nm^2 per each of the first three layers (see Figure S12). This result cannot be compared with experimental results on neither TiO_2 n-sh_NaOH nor TiO_2 n-sh_873K, where {001} surfaces are expected to be hydroxylated or (1x4) reconstructed, respectively. Nevertheless, an additional insight on the state of water on TiO_2 n-sh_873K in comparison with TiO_2 bipy was obtained by NIR spectroscopy (Figure 4B). The $\nu_{asym}+\delta(H_2O)$ band observed for TiO_2 bipy in equilibrium with 15 mbar H_2O (*i.e.* ~3 molecular layers of adsorbed water) is composed by a main absorption at ~5180 cm^{-1}, and a shoulder at ~5300 cm^{-1}, this latter due to the H-bonding free OH pointing towards the exterior of the upmost water layer.[44-45] This component accounts for ~3.7% of the overall integrated intensity, but this value increases to ~8.5% for H_2O on TiO_2 n-sh_873K. In agreement with the microgravimetric data, this feature should be related to

a decrease of the amount of water molecules underneath the upmost layer, i.e. a decreased number of H_2O layers on TiO_2 n-sh_873K.

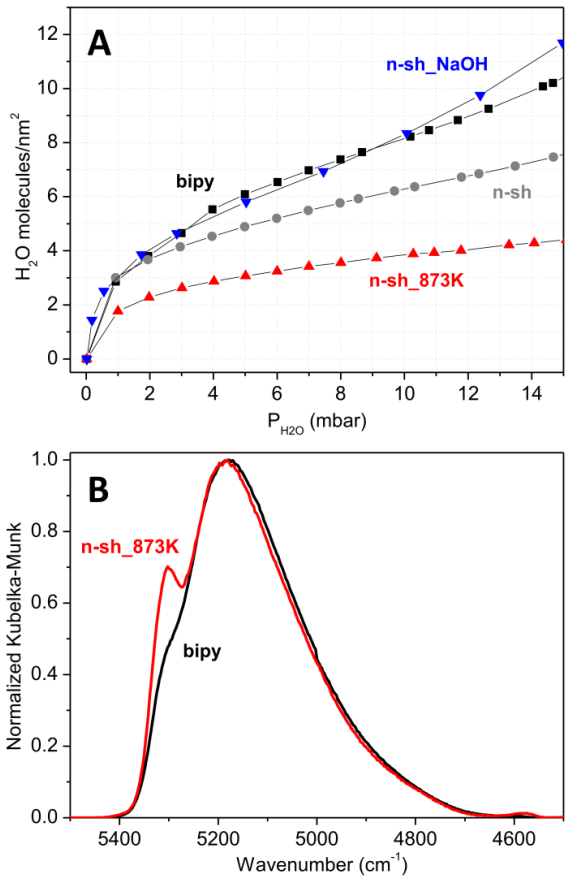

Figure 4. (A) Water adsorption isotherms at 298 K obtained from microgravimetric measurements. The samples have been previously outgassed at r.t. (B) Normalized NIR spectra of the TiO_2 bipy (black) and TiO_2 n-sh_873 K (red) samples in contact with H_2O at 15 mbar.

Information on the relative amount of water molecules left irreversibly adsorbed at r.t. on the various samples and on their hydroxylation state was provided by MIR spectroscopy. As a link with microgravimetric data (providing information on H_2O reversibly adsorbed at r.t.), also spectra of samples in contact with H_2O at 15 mbar were collected (Figure 5A). Relevant spectral features are: i) a weak, sharp band at ~3700 cm^{-1} due to the ν(OH) of H-bonding free H_2O molecules at the surface of the upmost water layer (see above), ii) an intense and broad absorption spread over the 3600-2800 cm^{-1} range, due to the ν(OH) of H-bonded water molecules and surface hydroxy groups, iii) the δ(H_2O)

signal of adsorbed H_2O molecules, with maximum at ~1635 cm^{-1}.[46-47] In addition, also the $\delta(H_2O)$ of water left adsorbed irreversibly by outgassing at r.t. is reported, for the sake of comparison (dashed lines). For each sample, the integral of the area between the full and dotted lines is proportional to the amount of reversibly adsorbed H_2O molecules. The relative values obtained (1.0/bipy, 0.7/n-sh, 0.9/n-sh_NaOH, 0.3/n-sh_873K) are in good agreement with those provided by microgravimetry (1.0/bipy, 0.7/n-sh, 1.1/n-sh_NaOH, 0.4/n-sh_873K). Thus, also the relative integrated intensity of the $\delta(H_2O)$ signals obtained for samples outgassed at r.t. (Figure 5B) should correspond to the relative amount of H_2O molecules left adsorbed in this condition, that was not possible to determine by microgravimetry. With respect to the pristine TiO_2 n-sh, the removal of fluorides by NaOH washing resulted in an increased capability of retaining water in the first hydration layer, becoming similar to that of TiO_2 bipy. Moreover, the upshift in position of the $\delta(H_2O)$ band indicates that a change in the interaction of water molecules with surface sites occurred, their behavior as H-bonding donors gaining in relative extent with respect to the interaction through the oxygen atom.[48-49] Noteworthy, the amount of water molecules retained by the surface of TiO_2 n-sh calcined at 873 K appears rather low. This well agrees with DFT calculations which suggested that, on the reconstructed (001) surface in the terrace region, water is physisorbed or not adsorbed at all.[16] Concerning the 3800-2700 cm^{-1} ν(OH) spectral profile of samples outgassed at r.t., TiO_2 bipy exhibits the well-known pattern made of a series of sharp bands at $\nu \geq 3600$ cm^{-1} due to isolated hydroxy groups, a band at 3470 cm^{-1} assigned to water molecules strongly coordinated with Ti^{4+} sites on {101}, overimposed to the onset of a broad absorption due to an extended network of hydrogen bonding between OH groups and water molecules.[46-47] This absorption becomes the dominant component of the ν(OH) profile of TiO_2 n-sh, at the expenses of signals due to isolated hydroxy groups. These signals are totally absent in the spectrum of TiO_2 n-sh_NaOH, indicating that the treatment in basic solution affected also the hydroxylation of {101} surfaces. Conversely, bands due to isolated OH are the main feature of the ν(OH) pattern of TiO_2 n-sh_873K, characterized by an overall weak intensity.

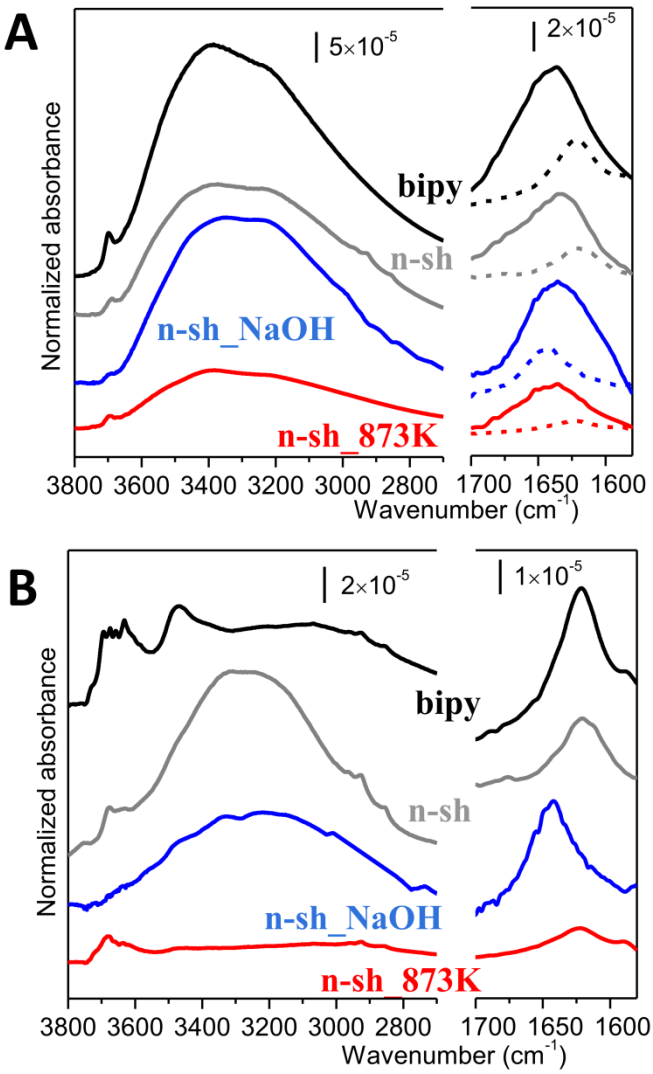

Figure 5. FT-IR spectra of the samples in contact with H_2O at 15 mbar (A) and after outgassing for 1 hour at r.t. (B). To facilitate the comparison, the spectra after outgassing for 1 hour are also reported in part (A) as dashed curves in the H_2O bending region. The spectral features of surface hydroxy groups and water molecules were extracted from original spectra as shown in Figure S14. The spectra here reported have also been normalized by dividing the absorbance by the specific surface area (m^2/g) and the "optical thickness" (g/m^2) of the pelletized samples.

3.4 Surface Lewis acidity

The Lewis acidity of surface Ti^{4+} sites was probed by IR spectroscopy of adsorbed CO.[50-51] This method requires the pre-outgassing at high temperature and, therefore, was applied only to TiO_2 n-sh_873K, that already experienced a thermal treatment, and to TiO_2 bipy, for the sake of comparison. Surprisingly, the main feature of the spectrum of CO adsorbed at ~100 K on TiO_2 n-sh_873K is the peak at ~2180 cm^{-1} due to probe molecules on {101} surfaces,[20, 52] similar in

position to the dominant peak of CO on TiO_2 bipy, whereas signals associated to {001} surfaces are not noticeable (Figure 6A). Details on the assignment of the other minor components are reported in Table S1 in the Supporting Information. By further decreasing the adsorption temperature down to ~60 K (Figure 6B) the dominant spectral feature of CO on TiO_2 n-sh_873K becomes a new band at ~2155 cm^{-1}, thus falling in a frequency range expected for CO adsorbed on Ti^{4+} sites on (1x4) reconstructed (001) surface as predicted by DFT calculations.[20] This band is fully reversible upon CO outgassing at 60 K, whereas the peak at ~2180 cm^{-1} remains almost unaffected (appearing reversible upon outgassing in the experiment at 100 K). Moreover, the maximum moves from ~2155 to ~2160 cm^{-1}, because of the fading away of adsorbate-adsorbate interactions, i.e. approaching the singleton ν(CO).[53] The very limited upshift of the singleton signal with respect to the stretching mode of CO in gas phase (2143 cm^{-1}) indicates that Ti^{4+} on such surfaces are rather weak as Lewis acid sites. This agrees with the weakness of their interaction with CO, actually scarce at a temperature as low as ~100 K.

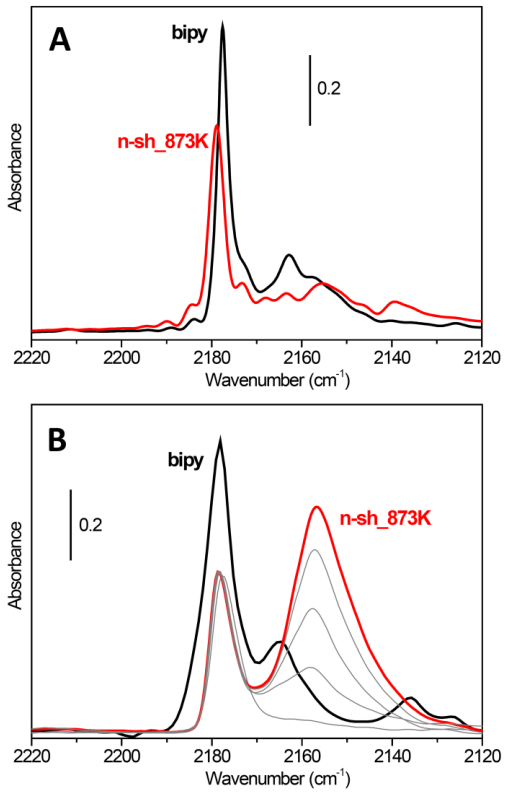

Figure 6. IR spectra of CO adsorbed on TiO_2 bipy (black) and TiO_2 n-sh_873 K (red) at 100 K (A) ad 60 K (B). In both cases, the sample was put in equilibrium with CO at 15 mbar at 100 K and then, for (B), the temperature was decreased to 60 K. The grey spectra in part (B) refer to progressive CO outgassing at 60 K for sample TiO_2 n-sh_873 K.

3.5 Photocatalytic activity

To investigate the impact of the differences in surface features between bare TiO_2 nanoparticles mainly terminated by {101} or (1x4) reconstructed {001} surfaces, TiO_2 bipy and TiO_2 n-sh_873K were tested in the phenol photodegradation reaction. The mechanism of phenol degradation has been widely studied demonstrating that for pure TiO_2 under UV irradiation $^{\cdot}OH$ radicals are the primary active species.[23] Recent studies highlighted the crucial role of both hydroxyls and adsorbed water in stabilizing the surface hole centers.[54] Moreover, also the amount of water adsorbed at the photocatalyst surface was found to strongly influence the efficiency of the phenol degradation process.[36] Thus, hydroxylation and surface affinity towards H_2O molecules are expected to have both a relevant influence on this process. For the sake of completeness, tests were carried out also for pristine TiO_2 n-sh and TiO_2 n-sh_NaOH, although the photocatalytic behavior of these nanoparticles should be affected also by the electronic states due to the presence of fluorides. Finally, we performed a test to further check that the thermal treatment at 873 K does not change the functional properties of TiO_2 bipy: in agreement with the morphological stability, already discussed in section 3.1, the photocatalytic activity does not significantly change between TiO_2 bipy and TiO_2 bipy_873K (see Figure S15).

Figure 7 shows the phenol photodegradation curves (panel A) and the related initial degradation rates (panel B), normalized by weight and specific surface area of the samples of nanoparticles. The effectiveness of TiO_2 n-sh_873 (red curve) in the phenol photodegradation is very limited, whereas TiO_2 bipy (black curve) appears significantly more active (*ca.* -6% and -23% of C_6H_5OH, respectively, after 180 min irradiation). Noteworthy, TiO_2 bipy has an initial degradation rate *ca.* 4.5 times higher than TiO_2 n-sh_873 K. Thus, the collection of data on surface features of these two types of nanoparticles allows to state that low hydrophilicity, poor hydroxylation, and weak Lewis acidity of Ti sites exhibited by reconstructed {001} surfaces affect negatively the photocatalytic performance of bare TiO_2 nano-sheet particles in the tested reaction with respect to the TiO_2 bipy ones, mainly exposing {101} facets.

As far as the other two forms of titania nano-sheet particles, TiO_2 n-sh and TiO_2 n-sh_NaOH, are concerned, they act as better photocatalysts in phenol degradation than TiO_2 n-sh_873K, in terms of both C_6H_5OH conversion along the duration of the test and initial rate. Interestingly, TiO_2 n-sh_NaOH nanoparticles, with surfaces freed from F^-, richer in hydroxy groups and more hydrophilic than pristine TiO_2 n-sh ones, are the most active, approaching the performance of TiO_2 bipy.

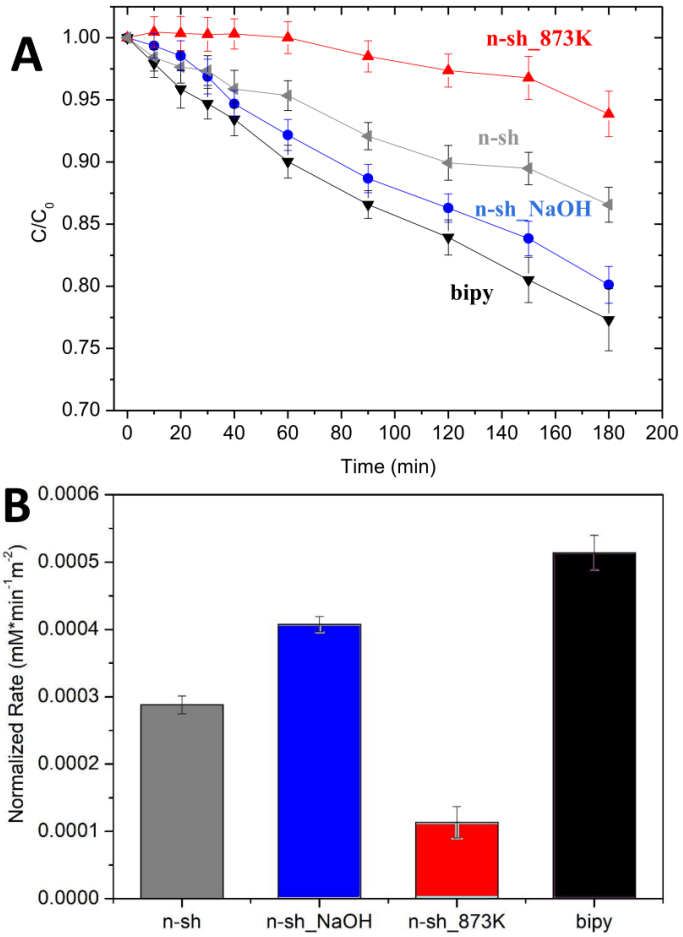

Figure 7. Phenol photodegradation curves (A) and related initial degradation rates, normalized by weight and specific surface area, (B) obtained using the various types of TiO_2 NPs.

4. Conclusions

The comprehensive set of data presented in this work leads to a main conclusion: TiO_2 nano-sheets exposing {001} facets as prevalent surfaces, prepared by capping with fluorides, can appear as particles similar in shape, but they actually show significant differences in surface/interfacial features, namely hydroxylation and hydrophilicity, in dependence on the treatment carried out (if any) for the

removal of F^- ions, which remain in the bulk and on the surface. Thus, other than obvious differences in electronic states due to these anions, also these aspects should be considered when evaluating functional properties involving surface/interfacial phenomena, as photocatalysis. Interestingly, a proper treatment in a basic solution of TiO_2 nano-sheets templated with fluorides allows to attain a complete exchange of surface F^- with OH^-, resulting in nanoparticles retaining the platy shape, and combining a high surface hydroxylation with the electronic states due to fluorides still retained in their bulk, as highlighted by XPS and UV-Vis spectroscopy. TiO_2 nano-sheets that underwent this treatment show an increase of 40% in normalized initial rate of phenol photodegradation with respect to pristine TiO_2 nano-sheets fluorinated both in the bulk and at the surface, which are also less hydroxylated and hydrophilic. Conversely, complete F^- elimination by calcination at 873 K results in a decrease of 60% in normalized initial rate with respect to pristine nanoparticles. The disappearance of electronic states due to F^- is accompanied by a significant decrease in surface hydroxylation and hydration, likely resulting from a (1x4) reconstruction of {001} facets.

Calcined TiO_2 nano-sheets, being free from both bulk and surface F^-, appear as the most suitable of the three types of platy-shaped TiO_2 nanoparticles, considered in this work, to be compared in a straightforward way with non-doped TiO_2 nanoparticles with different morphology. In this respect, (1x4) reconstructed {001} facets, mainly exposed by calcined TiO_2 nano-sheets, show significant lower hydrophilicity, poorer hydroxylation, and weaker Lewis acidity of Ti sites than {101} facets, mainly exposed by bipyramidal TiO_2 nanoparticles. These differences in surface features are accompanied by a normalized initial rate of phenol photodegradation 4.5 times lower for F^--free calcined TiO_2 nano-sheets.

Acknowledgements. The authors thank Markus Holzweber for assistance with ToF-SIMS measurements, Erik Ortel and Thomas Wirth for AES and ToF-SIMS analysis, Joerg Stockmann for XPS measurements, Chiara Deiana and Chiara Negri for support in the acquisition of the IR spectra.

This research was carried out in the frame of the FP7 European project SETNanoMetro - Shape-engineered TiO_2 nanoparticles for metrology of functional properties: setting design rules from material synthesis to nanostructured devices - (Project number 604577; www.setnanometro.eu), funded by EC.

Supporting Information. Details of the model adopted to calculate the expected specific surface area and percentage of exposed {001} surfaces; HR-TEM images of TiO_2 n-sh_NaOH; SEM/EDX, XPS, AES and ToF-SIMS data; Tauc plots; complete FT-IR spectra of the samples after outgassing for 1 hour at r.t.; phenol photodegradation curves for TiO_2 bipy and TiO_2 bipy_873K samples are available free of charge on the ACS Publications website.

References

((1) Chen, X.; Mao, S. S. Titanium Dioxide Nanomaterials: Synthesis, Properties, Modifications, and Applications. *Chem. Rev.* **2007,** *107*, 2891-2959.
(2) Hu, X. L.; Li, G. S.; Yu, J. C. Design, Fabrication, and Modification of Nanostructured Semiconductor Materials for Environmental and Energy Applications. *Langmuir* **2010,** *26*, 3031-3039.
(3) Liu, G.; Yu, J. C.; Lu, G. Q.; Cheng, H. M. Crystal Facet Engineering of Semiconductor Photocatalysts: Motivations, Advances and Unique Properties. *Chem. Commun.* **2011,** *47*, 6763-6783.
(4) Liu, J.; Olds, D.; Peng, R.; Yu, L.; Foo, G. S.; Qian, S.; Keum, J.; Guiton, B. S.; Wu, Z. L.; Page, K. Quantitative Analysis of the Morphology of {101} and {001} Faceted Anatase TiO_2 Nanocrystals and Its Implication on Photocatalytic Activity. *Chem. Mat.* **2017,** *29*, 5591-5604.
(5) Huang, M. H.; Naresh, G.; Chen, H. S. Facet-Dependent Electrical, Photocatalytic, and Optical Properties of Semiconductor Crystals and Their Implications for Applications. *ACS Appl. Mater. Interfaces* **2018,** *10*, 4-15.
(6) Yang, H. G.; Sun, C. H.; Qiao, S. Z.; Zou, J.; Liu, G.; Smith, S. C.; Cheng, H. M.; Lu, G. Q. Anatase TiO_2 Single Crystals with a Large Percentage of Reactive Facets. *Nature* **2008,** *453*, 638-641.
(7) Liu, S. W.; Yu, J. G.; Jaroniec, M. Anatase TiO_2 with Dominant High-Energy {001} Facets: Synthesis, Properties, and Applications. *Chem. Mat.* **2011,** *23*, 4085-4093.
(8) Shi, H. M.; Zhang, S.; Zhu, X. P.; Liu, Y.; Wang, T.; Jiang, T.; Zhang, G. H.; Duan, H. G. Uniform Gold-Nanoparticle-Decorated {001}-Faceted Anatase TiO_2 Nanosheets for Enhanced Solar-Light Photocatalytic Reactions. *ACS Appl. Mater. Interfaces* **2017,** *9*, 36907-36916.
(9) Ong, W. J.; Tan, L. L.; Chai, S. P.; Yong, S. T.; Mohamed, A. R. Highly Reactive {001} Facets of TiO_2-Based Composites: Synthesis, Formation Mechanism and Characterization. *Nanoscale* **2014,** *6*, 1946-2008.
(10) Gordon, T. R.; Cargnello, M.; Paik, T.; Mangolini, F.; Weber, R. T.; Fornasiero, P.; Murray, C. B. Nonaqueous Synthesis of TiO_2 Nanocrystals Using Tif_4 to Engineer Morphology, Oxygen Vacancy Concentration, and Photocatalytic Activity. *J. Am. Chem. Soc.* **2012,** *134*, 6751-6761.
(11) Minero, C.; Mariella, G.; Maurino, V.; Pelizzetti, E. Photocatalytic Transformation of Organic Compounds in the Presence of Inorganic Anions. 1. Hydroxyl-Mediated and Direct Electron-Transfer Reactions of Phenol on a Titanium Dioxide-Fluoride System. *Langmuir* **2000,** *16*, 2632-2641.
(12) Minero, C.; Bedini, A.; Maurino, V. Glycerol as a Probe Molecule to Uncover Oxidation Mechanism in Photocatalysis. *Appl. Catal. B-Environ.* **2012,** *128*, 135-143.
(13) Monllor-Satoca, D.; Gomez, R. Electrochemical Method for Studying the Kinetics of Electron Recombination and Transfer Reactions in Heterogeneous Photocatalysis: The Effect of Fluorination on TiO_2 Nanoporous Layers. *J. Phys. Chem. C* **2008,** *112*, 139-147.
(14) Minella, M.; Faga, M. G.; Maurino, V.; Minero, C.; Pelizzetti, E.; Coluccia, S.; Martra, G. Effect of Fluorination on the Surface Properties of Titania P25 Powder: An Ftir Study. *Langmuir* **2010,** *26*, 2521-2527.
(15) Maisano, M.; Dozzi, M. V.; Coduri, M.; Artiglia, L.; Granozzi, G.; Selli, E. Unraveling the Multiple Effects Originating the Increased Oxidative Photoactivity of {001}-Facet Enriched Anatase TiO_2. *ACS Appl. Mater. Interfaces* **2016,** *8*, 9745-9754.

(16) Selcuk, S.; Selloni, A. Surface Structure and Reactivity of Anatase TiO_2 Crystals with Dominant {001} Facets. *J. Phys. Chem. C* **2013,** *117*, 6358-6362.
(17) Yuan, W. T.; Wu, H. L.; Li, H. B.; Dai, Z. X.; Zhang, Z.; Sun, C. H.; Wang, Y. In Situ Stem Determination of the Atomic Structure and Reconstruction Mechanism of the TiO_2 (001) (1 X 4) Surface. *Chem. Mat.* **2017,** *29*, 3189-3194.
(18) Henderson, M. A. A Surface Science Perspective on TiO_2Photocatalysis. *Surf. Sci. Rep.* **2011,** *66*, 185-297.
(19) Mino, L.; Zecchina, A.; Martra, G.; Rossi, A. M.; Spoto, G. A Surface Science Approach to TiO_2 P25 Photocatalysis: An in Situ FTIR Study of Phenol Photodegradation at Controlled Water Coverages from Sub-Monolayer to Multilayer. *Appl. Catal. B-Environ.* **2016,** *196*, 135-141.
(20) Deiana, C.; Minella, M.; Tabacchi, G.; Maurino, V.; Fois, E.; Martra, G. Shape-Controlled TiO_2 Nanoparticles and TiO_2 P25 Interacting with CO and H_2O_2 Molecular Probes: A Synergic Approach for Surface Structure Recognition and Physico-Chemical Understanding. *Phys. Chem. Chem. Phys* **2013,** *15*, 307-15.
(21) Huang, Z. A.; Sun, Q.; Lv, K. L.; Zhang, Z. H.; Li, M.; Li, B. Effect of Contact Interface between TiO_2 and G-C_3N_4 on the Photoreactivity of G-C_3N_4/TiO_2 Photocatalyst: (001) Vs (101) Facets of TiO_2. *Appl. Catal. B-Environ.* **2015,** *164*, 420-427.
(22) Zhang, J.; Ma, X. M.; Zhang, L. L.; Lu, Z. D.; Zhang, E.; Wang, H. B.; Kong, Z.; Xi, J. H.; Ji, Z. G. Constructing a Novel N-P-N Dual Heterojunction between Anatase Tio_2 Nanosheets with Coexposed {101}, {001} Facets and Porous Zns for Enhancing Photocatalytic Activity. *J. Phys. Chem. C* **2017,** *121*, 6133-6140.
(23) Grabowska, E.; Reszczynska, J.; Zaleska, A. Mechanism of Phenol Photodegradation in the Presence of Pure and Modified-TiO_2: A Review. *Water Res.* **2012,** *46*, 5453-5471.
(24) Pellegrino, F.; Pellutie, L.; Sordello, F.; Minero, C.; Ortel, E.; Hodoroaba, V. D.; Maurino, V. Influence of Agglomeration and Aggregation on the Photocatalytic Activity of TiO_2 Nanoparticles. *Appl. Catal. B-Environ.* **2017,** *216*, 80-87.
(25) Han, X. G.; Kuang, Q.; Jin, M. S.; Xie, Z. X.; Zheng, L. S. Synthesis of Titania Nanosheets with a High Percentage of Exposed (001) Facets and Related Photocatalytic Properties. *J. Am. Chem. Soc.* **2009,** *131*, 3152-3153.
(26) Zhang, J. Y.; Wang, J. J.; Zhao, Z. Y.; Yu, T.; Feng, J. Y.; Yuan, Y. J.; Tang, Z. K.; Liu, Y. H.; Li, Z. S.; Zou, Z. G. Reconstruction of the (001) Surface of TiO_2 Nanosheets Induced by the Fluorine-Surfactant Removal Process under UV-Irradiation for Dye-Sensitized Solar Cells. *Phys. Chem. Chem. Phys.* **2012,** *14*, 4763-4769.
(27) Sugimoto, T.; Zhou, X. P.; Muramatsu, A. Synthesis of Uniform Anatase TiO_2 Nanoparticles by Gel-Sol Method 3. Formation Process and Size Control. *J. Colloid Interface Sci.* **2003,** *259*, 43-52.
(28) Martra, G.; Gianotti, E.; Coluccia, S. The Application of Uv-Visible-Nir Spectroscopy to Oxides. In *Metal Oxide Catalysis*, Wiley-VCH Verlag GmbH & Co. KGaA: 2009; pp 51-94.
(29) Yang, X. H.; Li, Z.; Sun, C. H.; Yang, H. G.; Li, C. Z. Hydrothermal Stability of {001} Faceted Anatase TiO_2. *Chem. Mat.* **2011,** *23*, 3486-3494.
(30) Mino, L.; Ferrari, A. M.; Lacivita, V.; Spoto, G.; Bordiga, S.; Zecchina, A. CO Adsorption on Anatase Nanocrystals: A Combined Experimental and Periodic DFT Study. *J. Phys. Chem. C* **2011,** *115*, 7694-7700.
(31) Ortel, E.; Hausler, I.; Osterle, W.; Narbey, S.; Oswald, F.; Andersen, I. H.; Holzweber, M.; Unger, W. E. S.; Hodoroaba, V. D. In-Depth Structural and Chemical Characterization of Engineered TiO_2 Films. *Surf. Interface Anal.* **2016,** *48*, 664-669.
(32) Czoska, A. M.; Livraghi, S.; Chiesa, M.; Giamello, E.; Agnoli, S.; Granozzi, G.; Finazzi, E.; Di Valentin, C.; Pacchioni, G. The Nature of Defects in Fluorine-Doped TiO_2. *J. Phys. Chem. C* **2008,** *112*, 8951-8956.
(33) Di Valentin, C.; Pacchioni, G.; Selloni, A. Reduced and N-Type Doped TiO_2: Nature of Ti^{3+} Species. *J. Phys. Chem. C* **2009,** *113*, 20543-20552.

(34) Biedrzycki, J.; Livraghi, S.; Giamello, E.; Agnoli, S.; Granozzi, G. Fluorine- and Niobium-Doped TiO_2: Chemical and Spectroscopic Properties of Polycrystalline N-Type-Doped Anatase. *J. Phys. Chem. C* **2014,** *118*, 8462-8473.
(35) Panayotov, D. A.; Burrows, S. P.; Morris, J. R. Infrared Spectroscopic Studies of Conduction Band and Trapped Electrons in UV-Photoexcited, H-Atom N-Doped, and Thermally Reduced Tio_2. *J. Phys. Chem. C* **2012,** *116*, 4535-4544.
(36) Mino, L.; Negri, C.; Zecchina, A.; Spoto, G. Photodegradation of Organic Pollutants on TiO_2 P25 Surfaces Investigated by Transmission FTIR Spectroscopy under in Situ UV-Vis Irradiation. *Z. Phys. Chem.* **2016,** *230*, 1441-1451.
(37) Bharti, B.; Kumar, S.; Lee, H. N.; Kumar, R. Formation of Oxygen Vacancies and Ti^{3+} State in TiO_2 Thin Film and Enhanced Optical Properties by Air Plasma Treatment. *Sci Rep* **2016,** *6*, 12.
(38) Jangir, M.; Jain, A.; Yamaguchi, S.; Ichikawa, T.; Lal, C.; Jain, I. P. Catalytic Effect of TiF_4 in Improving Hydrogen Storage Properties of MgH_2 *Int. J. Hydrogen Energy* **2016,** *41*, 14178-14183.
(39) Radnik, J.; Mohr, C.; Claus, P. On the Origin of Binding Energy Shifts of Core Levels of Supported Gold Nanoparticles and Dependence of Pretreatment and Material Synthesis **2003,** *5*, 172-177.
(40) Pan, J.; Liu, G.; Lu, G. M.; Cheng, H. M. On the True Photoreactivity Order of {001}, {010}, and {101} Facets of Anatase TiO_2 Crystals. *Angew. Chem.-Int. Edit.* **2011,** *50*, 2133-2137.
(41) Luca, V. Comparison of Size-Dependent Structural and Electronic Properties of Anatase and Rutile Nanoparticles. *J. Phys. Chem. C* **2009,** *113*, 6367-6380.
(42) Kavathekar, R. S.; Dev, P.; English, N. J.; MacElroy, J. M. D. Molecular Dynamics Study of Water in Contact with the TiO_2 Rutile-110, 100, 101, 001 and Anatase-101, 001 Surface. *Mol. Phys.* **2011,** *109*, 1649-1656.
(43) English, N. J. Diffusivity and Mobility of Adsorbed Water Layers at TiO_2 Rutile and Anatase Interfaces. *Crystals* **2016,** *6*, 1-7.
(44) Takeuchi, M.; Martra, G.; Coluccia, S.; Anpo, M. Investigations of the Structure of H_2O Clusters Adsorbed on TiO_2 Surfaces by near-Infrared Absorption Spectroscopy. *J. Phys. Chem. B* **2005,** *109*, 7387-7391.
(45) Schaefer, J.; Backus, E. H. G.; Nagata, Y.; Bonn, M. Both Inter- and Intramolecular Coupling of O-H Groups Determine the Vibrational Response of the Water/Air Interface. *J. Phys. Chem. Lett.* **2016,** *7*, 4591-4595.
(46) Deiana, C.; Fois, E.; Coluccia, S.; Martra, G. Surface Structure of TiO_2 P25 Nanoparticles: Infrared Study of Hydroxy Groups on Coordinative Defect Sites. *J. Phys. Chem. C* **2010,** *114*, 21531-21538.
(47) Mino, L.; Spoto, G.; Bordiga, S.; Zecchina, A. Particles Morphology and Surface Properties as Investigated by HRTEM, FTIR, and Periodic DFT Calculations: From Pyrogenic TiO_2 (P25) to Nanoanatase. *J. Phys. Chem. C* **2012,** *116*, 17008-17018.
(48) Soria, J.; Sanz, J.; Sobrados, I.; Coronado, J. M.; Maira, A. J.; Hernandez-Alonso, M. D.; Fresno, F. FTIR and NMR Study of the Adsorbed Water on Nanocrystalline Anatase. *J. Phys. Chem. C* **2007,** *111*, 10590-10596.
(49) Kevorkyants, R.; Rudakova, A. V.; Chizhov, Y. V.; Bulanin, K. M. The Origin of 1560 cm^{-1} Band in Experimental IR Spectra of Water Adsorbed on TiO_2 Surface: Ab Initio Assessment. *Chem. Phys. Lett.* **2016,** *662*, 97-101.
(50) Hadjiivanov, K. I.; Klissurski, D. G. Surface Chemistry of Titania (Anatase) and Titania-Supported Catalysts. *Chem. Soc. Rev.* **1996,** *25*, 61-69.
(51) Xu, M. C.; Gao, Y. K.; Moreno, E. M.; Kunst, M.; Muhler, M.; Wang, Y. M.; Idriss, H.; Woll, C. Photocatalytic Activity of Bulk Tio_2 Anatase and Rutile Single Crystals Using Infrared Absorption Spectroscopy. *Phys. Rev. Lett.* **2011,** *106*, 4.
(52) Mino, L.; Spoto, G.; Bordiga, S.; Zecchina, A. Rutile Surface Properties Beyond the Single Crystal Approach: New Insights from the Experimental Investigation of Different Polycrystalline Samples and Periodic DFT Calculations. *J. Phys. Chem. C* **2013,** *117*, 11186-11196.

(53) Hadjiivanov, K.; Reddy, B. M.; Knozinger, H. Ftir Study of Low-Temperature Adsorption and Co-Adsorption of ^{12}CO and ^{13}CO on a TiO_2-SiO_2 Mixed Oxide. *Appl. Catal. A-Gen.* **1999,** *188*, 355-360.
(54) Panarelli, E. G.; Livraghi, S.; Maurelli, S.; Polliotto, V.; Chiesa, M.; Giamello, E. Role of Surface Water Molecules in Stabilizing Trapped Hole Centres in Titanium Dioxide (Anatase) as Monitored by Electron Paramagnetic Resonance. *J. Photochem. Photobiol. A-Chem.* **2016,** *322*, 27-34.

TOC image